Phase Behavior of Nanoparticles Assembled by DNA Linkers

Huiming Xiong,[1] Daniel van der Lelie,[2] and Oleg Gang[1,*]

[1]*Center for Functional Nanomaterials, Brookhaven National Laboratory, Upton, New York 11973, USA*
[2]*Biology Department, Brookhaven National Laboratory, Upton, New York 11973, USA*

(Received 1 September 2008; published 8 January 2009)

The phase diagram of DNA linker mediated nanoparticle assemblies was experimentally investigated and constructed. Using small angle x-ray scattering we studied the dependence of the internal structure of assembly on two main system parameters: DNA linker length and the number of linkers per particle. The formation of a crystalline bcc phase was observed for a limited range of linker lengths, while the number of linkers per particle controlled the onset of system crystallization. The influence of linkage defects on crystalline structure was also examined.

DOI: 10.1103/PhysRevLett.102.015504 PACS numbers: 81.05.−t

The highly selective, reversible, and tunable properties of DNA hybridization provide an attractive platform for programmable self-assembly of objects on micro- and nanoscales [1–5]. In addition, the polymer nature of DNA allows for a variety of ways to modulate these interactions, for example, via steric repulsion [6,7]. Recent discoveries have revealed that a remarkable degree of order with body-centered cubic (bcc) and face-centered cubic (fcc) lattices can be obtained for DNA-mediated particle assemblies [8–10]. It was observed that the flexibility of the DNA linkage and the thermal pathway play important roles in the formation of the crystalline structures. Nevertheless, the phase behaviors, nature of the interaction potential, and the ordering mechanisms in these systems are far from being understood primarily due to the limited experimental realization.

One of the successful schemes to assemble DNA functionalized particles into superstructures utilizes a DNA linker, whose two ends are complementary to the respective mutually noncomplementary single stranded (ss) DNAs on the particles [8,10,11]. Both linker length L_n and number r of linkers per particle can determine the interparticle interactions [6] and the topology of linkages among particles [5,12], thus influencing the phase state. In this Letter we reveal how L_n and r, these two major system design parameters, can govern the formation of ordered phases in DNA driven particle assembly (Fig. 1). We demonstrate that the ordered phase exists only in a limited range of L_n, and that r effectively controls the onset of system crystallization. Moreover, by substituting both-end-active linker DNA with one-end complementary linker, called "neutral" DNA (Fig. 1), we probe the effects of linkage defects on the assembly process and resulting states.

The sets of systems containing mutually noncomplementary ssDNA functionalized gold nanoparticles (NP) of radius $R \approx 6$ nm and DNA linkers were prepared as previously reported [10]. Linkers of length L_n are composed of two 15 base recognition ends which are complementary to respective ssDNA tethered on particles AuNP-*A* and AuNP-*B*, plus a central flexible polythymine $(T)_n$ stretch of different lengths ($n = 0$, 15, 30, 70, 100, 130, and 170, denoted accordingly as *L*0, *L*15, *L*30, *L*70, *L*100, *L*130, and *L*170); the corresponding system is denoted as Sys-Ln. An equal mole of AuNP-*A* and AuNP-*B* are mixed with linkers at different linker/AuNP-*A* (or *B*) mole ratio r ($r = 8{:}1$, 12:1, 20:1, 36:1, 50:1, and 72:1, denoted as $r = 8, 12, 20, 36, 50, 72$, respectively) in 0.3 M PBS buffer (0.3 M NaCl, 10 mM phosphate buffer, pH ∼ 7.0), after which the mixture was incubated at 65 °C for 10 min, followed by cooling to room temperature for ∼2 h and annealing at 55 °C for 1 h. The typical measured hybridization efficiency for $r > 12$ is ∼70%–80%, inde-

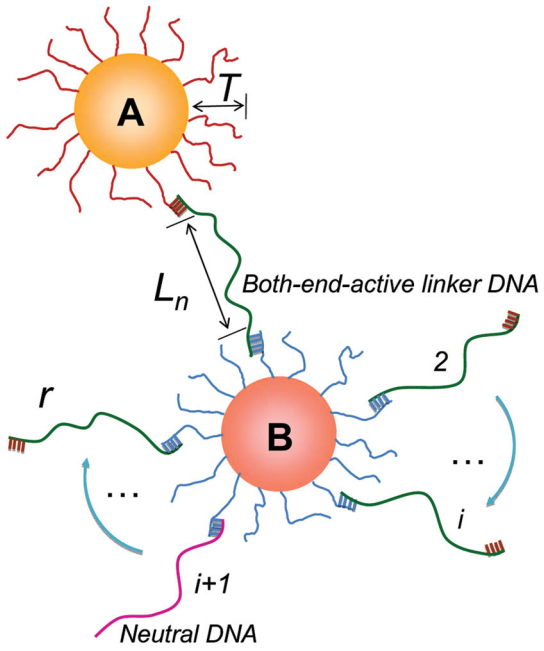

FIG. 1 (color). Schematics of particle-particle connections with DNA linkers of length L_n. Each particle connects with r linkers via hybridization with grafted ssDNAs. Linkers have both-end (active) or one-end (neutral) recognitions.

pendent of r and L_n as determined by UV-visible spectroscopy. We use a nominal r for data representation.

Synchrotron based small angle x-ray scattering (SAXS) technique (NSLS, beam line X21, 8 keV) was used to probe the structure of assembled aggregates. A typical 2D SAXS pattern of the crystal phase of an AuNP assembly, shown for Sys-L70 in Fig. 2(a), reveals 9 orders of resolution limited ($\Delta q_{\mathrm{res}} \approx 0.0012$ Å) diffraction peaks. Figure 2(b) summarizes structure factors $S(q)$ of Sys-Ln with n varied from 0 to 170 at $r = 36$. We found that Sys-L0 and Sys-L170 exhibited a limited number of broad peaks, characteristic of a disordered state. In contrast, all other systems (Sys-L15, Sys-L30, Sys-L70, Sys-L100, and Sys-L130) show sharp Bragg's peaks, with positions revealing a ratio $q/q_1 = 1{:}2^{1/2}{:}3^{1/2}{:}4^{1/2}{:}5^{1/2}{:}6^{1/2}{:}7^{1/2}$ up to at least seven orders, which correspond to {110}, {200}, {211}, {220}, {310}, {222}, and {321} crystalline planes in the bcc unit cell. For systems with linkers longer than L_{70} a peak broadening is observed, which indicates a decreased correlation length. The tendency of a longer linker to decrease system order is eventually manifested in the transition to the disorder phase as observed for Sys-L170.

The well-defined crystalline structures of systems with linker length ranging L_{15} to L_{130} allow one to quantify the evolution of particle surface-to-surface distance $D = \sqrt{3}a/2 - 2R$ as a function of n using obtained lattice constants a. D monotonically increases from ~19 to ~31 nm for a corresponding increase of linker length from L_{15} to L_{130}, as is shown in Fig. 2(c). To estimate this dependence we express $D = R_{ee} + 2T$, where R_{ee} is the end-to-end distance of the central flexible polythymine stretch of the DNA linkers approximated by worm-chain model as $R_{ee} = \sqrt{2l_pL[1 - \frac{l_p}{L}(1 - e^{-L/l_p})]}$, and T is a characteristic length of 30 base ssDNAs tethered on AuNPs, estimated according to Daoud-Cotton blob model [13] as $T = R[(1 + k\frac{Lc}{R}(\frac{\sigma\nu}{l_k})^{1/3})^{3/5} - 1]$, where $L_c = Nb$ is the contour length of ssDNA consisting of N nucleotides of segment length b. Here, $L_c = 19.5$ nm for 30 base ssDNA attached to particle surface; $l_k = 2l_p$ (persistence length $l_p \sim 1$ nm) is the Kuhn length of ssDNA; tethering density $\sigma = 0.145$ chains/nm^2 is calculated based on estimation of ~60 ssDNA on a particle which is measured as reported [14]; k is a constant on the order of unity. The excluded volume parameter ν can be approximated according to Onsager's concept as $\nu = 1.5l_k^2 d_{\mathrm{eff}}$, in which ssDNA chain can be viewed as a chain of charged cylinders with a length of ssDNA Kuhn length and effective diameter d_{eff} of ssDNA (~1 nm) plus twice the Debye screening length κ^{-1}. For quenched salted polyelectrolyte brushes in our case, with added salt concentration $C_a = 0.3$ M, $\kappa^{-1} \approx 0.3046C_a^{-1/2} = 0.57$ nm, $d_{\mathrm{eff}} = 2.14$ nm. The evaluated DNA shell thickness $T \sim 8$ nm reasonably correlates with ~6 nm deduced from hydrodynamic diameter of DNA functionalized particles measured by using dynamic light scattering [10]. Figure 2(c) (red line) illustrates a fit of the dependence of D on linker length L_n using the worm-chain model with one free fit parameter, l_p, and $T = 6$ nm. The obtained value of $l_p \sim 2.1$ nm for ssDNA agrees with the reported 2.2 nm at this salt concentration, measured by fluorescence resonance energy transfer method [15]. However, we emphasize that this somewhat elevated magnitude compared to other results [16], ~1 nm, might also indicate a collectively increased rigidity of ssDNA linkers. This effect can be associated to a chain entropy loss due to orientation confinement of linkers along the axis crossing centers of connected particles.

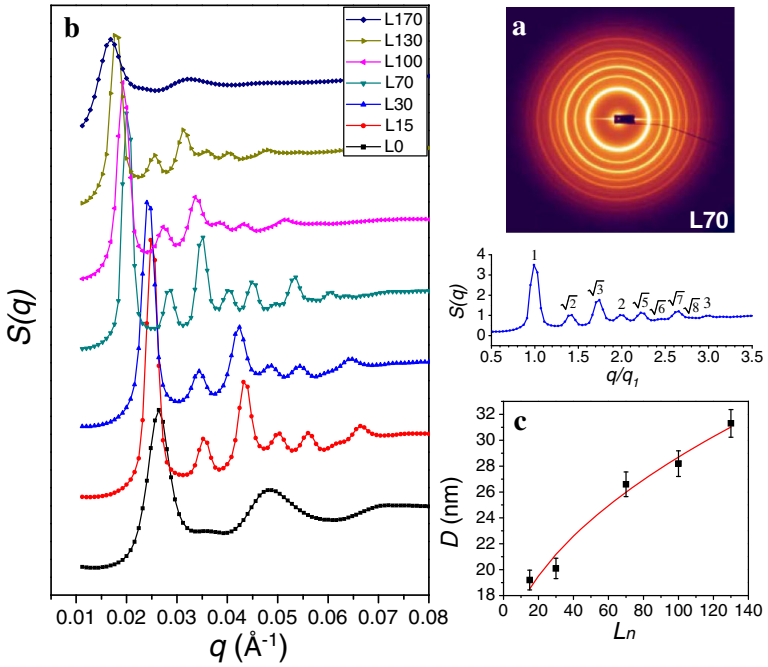

FIG. 2 (color online). (a) SAXS pattern of Sys-L70 and its structure factor $S(q)$ vs q/q_1. (b) $S(q)$ of annealed systems of different L_n ($n = 0$, 15, 30, 70, 100, 130, and 170 bottom up) at linker/AuNP ratio $r = 36$. (c) Interparticle surface-to-surface distance D vs L_n.

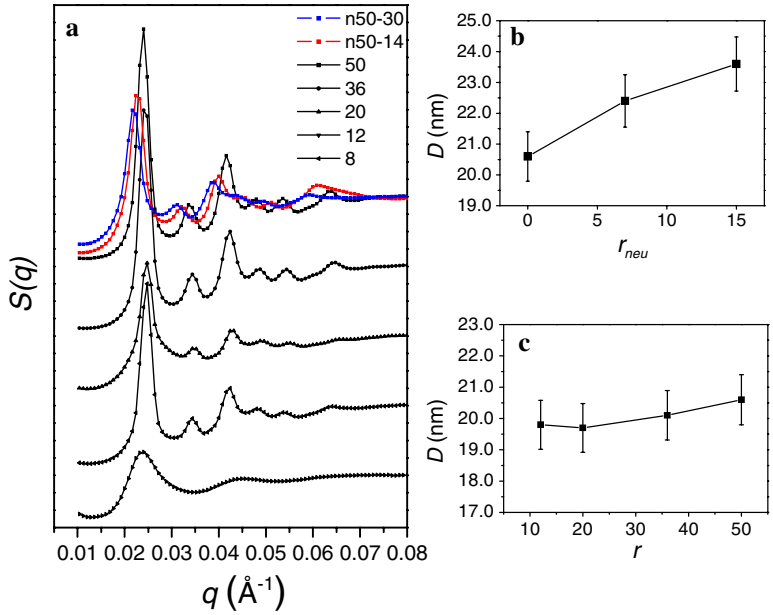

FIG. 3 (color online). (a) $S(q)$ of Sys-L30 at regular linker/neutral DNA/AuNP ratios equal to 20:30:1 (n50-30), 36:14:1 (n50-14), and 50:0:1 ($r = 50$), and different regular linker/AuNP ratios r. (b) Change of interparticle surface-to-surface distance D with number of neutral DNA per particle r_{neu}. (c) The dependence of D on r.

Although each nanoparticle might have up to r connections with particles in the first coordination shell, it is advantageous to know whether both ends of the linker simultaneously hybridize with complementary ssDNAs on the AuNPs, and what the effect of reduced efficiency of interparticle hybridization, caused by linkage ''defects,'' will have on the crystal structure. To address this, we introduced neutral DNAs with only one recognition end complementary to the respective ssDNAs on the AuNPs. The effect was studied for Sys-L30 at $r = 50$ by providing a mixing ratio of regular linker/neutral DNA/AuNP equal to 36:14:1, 20:30:1 (denoted as n50-14 and n50-30, respectively), and 50:0:1 (no neutral DNA).

Surprisingly, we observed that all these systems assembled in a crystalline order with bcc unit cell, as their corresponding $S(q)$ are shown in Fig. 3(a). Progressive broadening of diffraction peaks upon increased fraction of neutral DNA is observed, with decreasing correlation length of the first peak, from 460 to 260 to 240 nm for n50, n50-14, and n50-30. The interparticle distances are also systematically increasing from 32.1 to 33.9 and to 36 nm, correspondingly, which are 3.9 and 2.3 nm larger than those of systems $r = 36$ and $r = 20$ having the same ratio of regular linkers without neutral DNA, respectively. This result clearly illustrates that introduction of a small amount of neutral DNA has a significant effect on the interparticle distances, which is attributed to the steric repulsion between unhybridized ssDNAs acting as polyelectrolyte polymer brushes [6]. In another respect, this significant change reflects the structural plasticity of this intrinsically weak solid.

We also systematically varied the r value to probe how allowable connectivity affects coordination number and the resulting phase. Figure 3 summarizes the SAXS results for Sys-L30 as a representative case. It is found that transition to a crystalline phase occurs above a minimum r. For Sys-L30 at nominal $r = 8$, only the disordered phase is observed as indicated by broad liquidlike $S(q)$. Upon r increases to $r \sim 12$ and higher, resolution limited diffraction peaks appear with positions corresponding to the bcc lattice. Only a slight increase of D (<1 nm) is observed when r was varied from 12 to 50 [Fig. 3(c)]. The weak dependence on r, combined with a much larger D dependence on the fraction of neutral DNA [Fig. 3(b)] points to a high efficiency of simultaneous hybridization of both linker ends to NP. Interestingly, higher onset values of r for crystallization were observed for systems with longer linkers. For example, Sys-L70 exhibits an onset value for crystallization at $r \sim 20$, while for Sys-L130 this is at $r \sim 36$. Sys-L170 does not form a crystalline structure, it only exhibits a slight increase of correlation length at nominal $r = 72$, which is marked at $r = 60$ due to the saturation of the total number ($\sim$60) of available sites on the NP.

To parametrize the observed behavior a phase diagram was built in a way similar to star polymer systems [17]. In our case, we define the particle volume fraction η as $8\pi(R + T)^3/3(a)^3$ in bcc lattice, and r is analogous to so-called functionality [17]. Thus, the assembled systems can be envisioned as core-shell NPs connected by r stretchable springlike DNA linkers, whose lengths determine η. Figure 4 illustrates the measured phase diagram (η, r) for DNA linker mediated particle assemblies at room temperature as determined after thermal annealing. It is worth noting that at the annealing temperature where the system is close to equilibrium, the DNA linkages reform reversibly, and the particles are still collectively connected. For Sys-L30, a bcc phase is detected for $r > 8$. Remarkably, taking into account the hybridization efficiency, the initial manifestation of bcc at $r \sim 12$ agrees with a requirement on a coordination number to be equal to 8 for establishing nearest neighbor connections in the bcc lattice. The consequent η decrease with increasing L_n results in a corre-

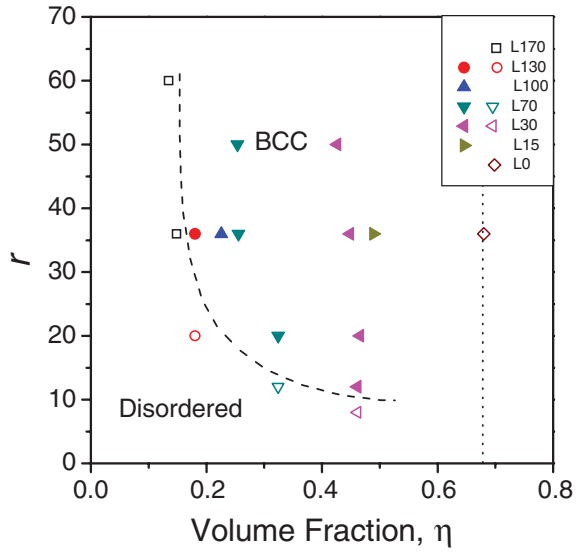

FIG. 4 (color). Experimental phase diagram of NPs in terms of nominal linker/AuNP ratio r and volume fraction η. The dashed line is the boundary condition drawn for a guide to the eyes. Open symbols and solid symbols correspond to disordered and ordered states, respectively. Vertical dotted line represents maximum volume fraction of bcc phase of touching core-shell NPs.

sponding shift of the onset of crystallization to larger r. Eventually, at $\eta_{\min} \sim 0.18$, the number of linkers r required for ordering exceeds the number of sites on a particle, which determined the lowest η in bcc phase boundary. The appearance of bcc phase for the range $0.18 < \eta < 0.5$ maps surprisingly well with the calculated phase behavior of star polymers, dominated in this regime by the Yukawa potential [17]. DNA induced ordering requires considerably lower minimum number, $r_{\min} \sim 8$, compared to $r_{\min} = 34$ for star polymers, which is possibly due to the hybridization driven mechanism of assembly and establishment of bridges among particles.

Our previously reported experiments [9,10] indicate that the transition to ordering occurs close to melting temperature. We hypothesize that the presence of dynamically unhybridized linker DNAs at those temperatures allows for particle repositioning and may also provide additional repulsion scalable with distances between next neighbors. As the linker length increases, the spring constant $K = 3k_BT/2L_cl_p$ of linker coils decrease as $1/N$, which results in a potential softening [18]. Consequently, this diminishes a free energy difference between ordered and disordered states. Mechanistically, reduced K will permit larger amplitude of particle thermal fluctuation, and lead to random packing. This will suppress an onset of crystalline phase for smaller η, i.e., larger L_n. In accordance with the experimental observation, the reduced energy difference can be possibly compensated by increasing the number r of molecular springs. The observed transition to ordered phase for larger r could be related to recent findings [19–22] that revealed an increase of the melting temperature of the condensed phase with an increase of the number of interparticle bonds due to the effect of entropic cooperativity in the DNA-particle assemblies [19]. Nevertheless, theoretical descriptions that will account for interplay of interactions, bonding dynamics, and topology of interparticle connections are called for to shed light on the microscopic mechanism of phase formation in DNA-mediated nanosystems.

In summary, we investigated in detail the phase behavior of nanoparticle systems assembled by using a DNA linker strategy. We observed that two major system design parameters, DNA linker length and number r of linkers per particle, determined the transition from disordered to crystalline bcc phase. The order-disorder phase boundary shifts to higher r for longer linkers, and the eventual manifestation of the disordered state occurs when r exceeds the number of attachment sites on a particle.

Research was supported by the U.S. DOE Office of Science and Office of Basic Energy Sciences under Contract No. DE-AC-02-98CH10886.

*ogang@bnl.gov

[1] C. A. Mirkin *et al.*, Nature (London) **382**, 607 (1996).
[2] A. P. Alivisatos *et al.*, Nature (London) **382**, 609 (1996).
[3] J. P. Zhang, Y. Liu, Y. G. Ke, and H. Yan, Nano Lett. **6**, 248 (2006).
[4] P. L. Biancaniello, A. J. Kim, and J. C. Crocker, Phys. Rev. Lett. **94**, 058302 (2005).
[5] D. B. Lukatsky, B. M. Mulder, and D. Frenkel, J. Phys. Condens. Matter **18**, S567 (2006).
[6] A. V. Tkachenko, Phys. Rev. Lett. **89**, 148303 (2002).
[7] M. P. Valignat *et al.*, Proc. Natl. Acad. Sci. U.S.A. **102**, 4225 (2005).
[8] S. Y. Park *et al.*, Nature (London) **451**, 553 (2008).
[9] D. Nykypanchuk, M. M. Maye, D. van der Lelie, and O. Gang, Nature (London) **451**, 549 (2008).
[10] H. M. Xiong, D. van der Lelie, and O. Gang, J. Am. Chem. Soc. **130**, 2442 (2008).
[11] S. J. Park *et al.*, J. Phys. Chem. B **108**, 12375 (2004).
[12] J. Largo, F. W. Starr, and F. Sciortino, Langmuir, **23**, 5896 (2007).
[13] R. Hariharan, C. Biver, J. Mays, and W. B. Russel, Macromolecules, **31**, 7506 (1998).
[14] M. M. Maye, D. Nykypanchuk, D. van der Lelie, and O. Gang, J. Am. Chem. Soc. **128**, 14020 (2006).
[15] M. C. Murphy *et al.*, Biophys. J. **86**, 2530 (2004).
[16] S. B. Smith, Y. J. Cui, and C. Bustamante, Science **271**, 795 (1996).
[17] M. Watzlawek, C. N. Likos, and H. Löwen, Phys. Rev. Lett. **82**, 5289 (1999).
[18] M. Rubinstein and R. H. Colby, *Polymer Physics* (Oxford University, New York, 2003).
[19] D. B. Lukatsky and D. Frenkel, Phys. Rev. Lett. **92**, 068302 (2004).
[20] S. Y. Park and D. Stroud, Phys. Rev. B **67**, 212202 (2003).
[21] R. C. Jin *et al.*, J. Am. Chem. Soc. **125**, 1643 (2003).
[22] Y. Sun, N. C. Harris, and C. H. Kiang, Physica (Amsterdam) **354A**, 1 (2005).